Biosensors and Bioelectronics 218 (2022) 114749

Contents lists available at ScienceDirect

Biosensors and Bioelectronics

journal homepage: www.elsevier.com/locate/bios

An electronic nose based on 2D group VI transition metal dichalcogenides/organic compounds sensor array

Sara Gaggiotti [a,b,1], Annalisa Scroccarello [a,1], Flavio Della Pelle [a,*], Giovanni Ferraro [c], Michele Del Carlo [a], Marcello Mascini [a], Angelo Cichelli [b], Dario Compagnone [a,**]

[a] Faculty of Bioscience and Technology for Food, Agriculture and Environment, University of Teramo, Campus "Aurelio Saliceti" Via R. Balzarini 1, 64100, Teramo, Italy
[b] Department of Science, University of Pescara-Chieti, Viale Pindaro 42, 65127, Pescara, Italy
[c] Department of Chemistry "Ugo Schiff" and Consorzio per lo Sviluppo dei Sistemi a Grande Interfase (CSGI), University of Florence, Via Della Lastruccia 3-Sesto Fiorentino, I-50019, Florence, Italy

ARTICLE INFO

Keywords:
Gas sensors
Nanomaterials
Liquid-phase exfoliation
van der Waals materials
Polyphenols
Volatile organic compounds

ABSTRACT

Rapid volatile organic compounds (VOCs) detection is a hot topic today; in this framework nanomaterials and their tailorable chemistry offer a plethora of compelling opportunities. In this work, Group VI transition metal dichalcogenides (TMDs, i.e., MoS_2, WSe_2, $MoSe_2$, and WSe_2) were functionalized with organic compounds (ellagic acid, tannic acid, catechin, and sodium cholate) able to assist their sonochemical exfoliation in water. The 16 resulting water-dispersed 2D hybrid inorganic/organic TMDs resulted in a few-layer nanoflakes conformation and were used to modify quartz crystal microbalances (QCMs) to equip an e-nose for VOCs determination. The ability of the sensors for the detection of VOCs was assessed on alcohols, terpenes, esters, and aldehydes; the responses were significatively different, confirming the synergic effect of TMD and the organic compound in the interaction with VOCs. The 16 sensors exhibited quantitative responses for VOCs ($R^2 \geq 0.978$) with fast signals recovery (<100 s) and repeatable (RSD ≤9.3%, n = 5), reproducible (RSD ≤12.8%, n = 3) and stable (RSD ≤14.6%, 3 months) signals. As proof of applicability, in an e-nose format, banana aroma evolution during post-harvest ripening was successfully monitored using the 2D TMDs-based sensors array. These data demonstrate that TMDs exfoliated in water with different organic compounds are sustainable functional nanomaterials, able to offer new opportunities in nano-bioelectronic applications.

1. Introduction

Rapid volatile organic compounds (VOCs) detection and discrimination is of primary interest in modern society for monitoring environmental pollutants, identifying safety and process markers in food, and also for non-invasive medical diagnostics (Wang, 2020). Therefore, the development of high-performance gas sensors (GSs) is increasingly relevant in this multidisciplinary research area.

The performance of a GS is closely related to the detection mechanism that is governed by the surface reaction/interaction taking place among the target gas molecules and the surface of the sensing layer. In order to improve sensitivity and selectivity, often biological or biomimetic elements have been used as receptors, particularly on QCMs taking advantage of the possibility to work at room temperature. Olfactory binding protein (OBP) (Sayago et al., 2019), insect antennae (Paczkowski et al., 2015), porphyrins (D'Amico et al., 2000), peptides (Gaggiotti et al., 2020; Mascini et al., 2018; Mascini et al., 2017) DNA (Hairpin-DNA) (Gaggiotti et al., 2019; Marcello Mascini et al., 2019), and molecular imprinting polymers (MIPs) (Brenet et al., 2018; Gaggiotti et al., 2020) are key elements in this respect. On the other hand, several advances have been made regarding the direct use of functional nanomaterials as reliable and robust gas sensing elements.

Two-dimensional layered materials, with graphene as the headliner, have changed the sensor's field. In the last years, new 2D layered materials, boosted material research giving rise to innovative devices able to allow cutting-edge applications. Among these, transition metal dichalcogenides (TMDs), black phosphorene, and MXenes resulted particularly appealing for biosensoristic purposes (Kumar et al., 2020;

* Corresponding author.
** Corresponding author.
E-mail addresses: fdellapelle@unite.it (F. Della Pelle), dcompagnone@unite.it (D. Compagnone).
[1] These authors contributed equally.

https://doi.org/10.1016/j.bios.2022.114749
Received 3 June 2022; Received in revised form 8 September 2022; Accepted 22 September 2022
Available online 26 September 2022

Rojas et al., 2022). In particular, TMDs exhibit tunable dimensions and thickness, large surface-to-volume ratio, ease of surface functionalization, high compatibility for device integration, as well as peculiar mechanical and electronic/electroanalytical properties; thus, they are particularly appealing as sensing elements or sensing element supports (Samadi et al., 2018).

The exfoliation phenomenon of TMDs consists in providing energy to win interactions among layers, stabilizing the exfoliated sheets via solvent or stabilizing agents, to obtain a nanostructured material (Grayfer et al., 2017). Few-layer nanosheets can be obtained via chemical synthesis, chemical vapor deposition, and exfoliation using mechanical and chemical strategies; among the latter, Liquid Phase Exfoliation (LPE) is the most useful for mass production (Samadi et al., 2018). Production of TMDs colloidal nanosheets' in water using different stabilizing agents has been recently demonstrated; the stabilization of the nanosheets occurs, in this case, mainly through non-covalent interactions (Grayfer et al., 2017). Interesting features can be conferred by selecting a proper stabilizing agent, that remains anchored on the surface of the 2D nanosheet. Recently, in the frame of sustainability and green research goals (UN General Assembly, 2015), biological and natural products have been used for 2D layered material exfoliation in water (Paredes and Villar-Rodil, 2016; Silveri et al., 2021), demonstrating the ability to work as stabilizer agents and, at the same time, add useful features to the nanomaterial (Silveri et al., 2021, 2022).

TMDs, particularly MoS_2 and WS_2, have been widely used in chemoresistive-type and field-effect transistor gas sensors, because of their electrical capacity, low power consumption, large specific surface areas, and peculiar surface activity, as well as technological compatibility (Ghatak et al., 2011; Ko et al., 2016; Wang et al., 2012; Zhang et al., 2021). On the other hand, despite different piezoelectric quartz crystal microbalances (QCMs)-based gas sensors using graphene and graphene oxide as sensitive materials have been reported (Fauzi et al., 2021), just one study concerning MoS_2 is present in the literature. A MoS_2/VS_2 heterostructure has been engineered and tested onto a QCM in static conditions; a quite long (about three days) and complex two-step hydrothermal method was used to synthesize the MoS_2/VS_2 heterostructure composed of MoS_2 nanosheets vertically grown on a porous VS_2 scaffold. Interestingly, the sensor had a strong affinity for ammonia (Zhang et al., 2020). To the best of our knowledge, there are no comprehensive studies regarding the direct use of TMDs to functionalize/boost piezoelectric sensors. Moreover, in our opinion, TMDs obtained via water-phase exfoliation by bio/natural stabilizing agents deserve to be studied as gas receptors, since straightforward, sustainable and potentially able to modulate interaction with VOCs.

In this work, Group VI TMDs (i.e., MoS_2, $MoSe_2$, WS_2, and WSe_2) were obtained and functionalized via LPE with natural phenols (ellagic acid, tannic acid, and catechin) and sodium cholate. The obtained TMDs nanosheets have been characterized and challenged for the first time as sensing materials in piezoelectric gas sensors towards different VOC classes. The 16 TMDs-based sensors have been employed to equip a QCM-based e-nose; alcohols, esters, aldehydes, and terpenes have been tested as analytes. The repeatability, stability, and ability to return quantitative results have been proved. Finally, the recognition ability of a TMDs-equipped e-nose in real samples was demonstrated monitoring the aroma evolution of bananas (*Musa acuminata*) during post-harvest ripening. As expected, the TMDs' sensing ability is modulated by the nanomaterial chemistry and by the organic compounds used for the exfoliation.

2. Experimental

2.1. Chemicals, samples and apparatus

A detailed description of the chemicals, samples, and apparatus employed is reported in the Supporting Information. For simplicity, the TMDs have been generically called MX_2, where M = Mo or W and X = S or Se.

2.2. TMDs exfoliation and QCMs-MX_2 preparation

The liquid phase exfoliation of MoS_2, WS_2, $MoSe_2$, and WSe_2 has been carried out in water using ellagic acid (*El*), tannic acid (*Tn*), catechin (*Ct*), and sodium cholate (*Ch*) as stabilizing agents.

Briefly, the bulk TMD powder was exfoliated placing 500 mg of material in 50 mL of water containing 1 mg mL^{-1} of the organic compound. The TMDs were roughly dispersed with a bath sonicator (5 min), placed in a steel beaker, and sonicated with a Branson SFX550 Probe Sonifier for 5 h at 50% of amplitude (2 s on, 1 s off; probe Ø 13 mm). The exfoliated TMDs dispersion was then centrifuged at 250 g (1 h) to remove the material not properly exfoliated the supernatant was further centrifuged at 20,000 g for 15 min. The pellet containing the MX_2 nanosheets was resuspended in 50 mL of Milli-Q water and the exfoliation yield was calculated by gravimetry. All the MX_2 dispersions were brought to 50 mg mL^{-1}.

The 20 MHz QCM sensor functionalization was achieved by drop-casting 40 μL of MX_2 dispersion (four depositions of 5 μL for each side of the QCM) using a 20 W warm lamp to accelerate drying. Before use, the QCM-MX_2 sensors were washed with abundant Milli-Q water and let completely dry under N_2 (2 L h^{-1}).

2.3. Measurement setup

The QCM-MX_2 sensors were placed in an E-nose UTV (Sensor group, University of Rome, Tor Vergata) able to house 12 QCMs; the piezoelectric sensors are placed in a sealed measuring chamber, equipped with a release valve for gases output. For all the measurements, N_2 at a flow rate of 2 L h^{-1} was employed. To test the 16 QCM-MX_2 sensors, the measurements were run twice using 8 QCM-MX_2 sensors +1 bare QCM each time; each measure was performed in triplicate.

For VOCs analysis, the VOC standard/sample was placed in a gas-tight lab bottle (100 mL) placed at 40 °C, used as an evaporation/accumulation chamber; the latter communicates with a gas-tight loop through a gas-tight three-way polycarbonate valve (TW-valve). The VOCs accumulation time was set at 15 min; during this time, the loop inlet valve is open filling the loop. The switch of the TW-valve inlet and outlet allows N_2 to carry the VOCs into the measurement chamber. The frequency shifts (ΔF) were recorded and used as analytical signals. In Scheme 1 is reported the measuring set-up.

VOC dose-response curves were obtained using as loops PVC gas tights tubes with the same diameter (Ø 3 mm) and different lengths (from 5 cm to 160 cm). In this case, an estimation of the VOCs concentration was obtained according to She et al. (2021) with some modification, saturating the loops with a known amount of VOCs at a controlled temperature (40 °C).

For sample analysis, 3 g of banana was peeled-off and cut into cubes of approximately 1 cm^2, inserted in the gas-tight lab bottle equipped with an 80 cm loop. After 15 min of accumulation at 40 °C, the measurement was performed. The banana post-harvesting evolution was monitored by measuring bananas stored at room temperature, each day for 10 days. In this case, the responses returned by the QCM-MX_2 array were analyzed by unsupervised multivariate techniques using XLSTAT software (Addinsoft, New York, NY) for the principal component analysis (PCA) datasets were auto-scaled (zero mean and unitary variance) before analysis.

3. Results and discussion

3.1. 2D MX_2 production assisted by organic compounds

To exfoliate the four selected TMDs in 2D nanosheets modulating at the same time their surface chemistry, LPE in water-phase was strategically used taking advantage of the functional role of El, Tn, Ct, and Ch.

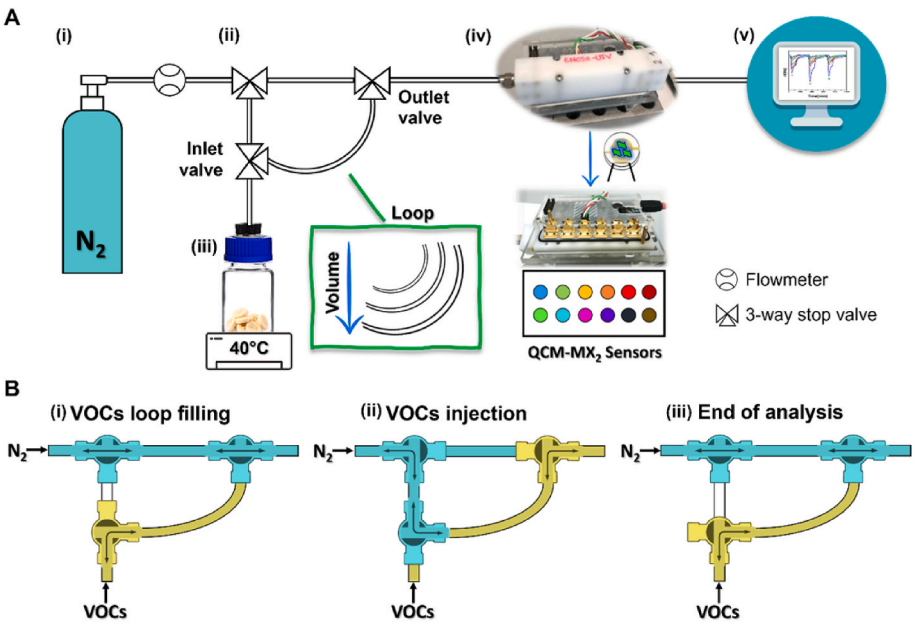

Scheme 1. (**A**) E-nose measurement set-up. (i) Carrier gas, (ii) loop/valves sampling system, (iii) sample chamber, (iv) measuring chamber equipped with QCM-MX_2 sensors, (v) acquisition interface and analysis software. (**B**) Loop/valves system working mode. (i) N_2-flow direct to measuring chamber - loop filling with VOCs coming from the sampling chamber; baseline formation. (ii) N_2-flow switched to carry the VOCs sampled by the loop to the measurement chamber; variation of the signal due to the interaction of the VOCs with the sensors (iii). Restoring of the N_2-flow to the initial position, exclusion of the loop; baseline recovery.

Recently, we have demonstrated the selected organic compounds' ability to successfully assist the LPE, conferring at the same time different functionalities to the obtained 2D nanoflakes (Rojas et al., 2022). The rationale behind the experimental hypothesis was to prove how different 2D hybrid inorganic/organic nanomaterials may exhibit different VOCs detection abilities because of the different core and surface chemistry conferred by the TMD and the organic compound, respectively.

A detailed description of the procedure for MX_2 nanosheets production is given in *section 2.2*. In the LPE process, the ultrasounds allow layers and size reduction of the bulk-TMD, and the organic compound stabilizes the MX_2 nanosheets.

The carbon skeleton of the organic compounds used for the exfoliation allows structural non-covalent interactions with MX_2 nanosheets (Rojas et al., 2022; Silveri et al., 2021). In the case of sodium cholate (Ch), the rigid structure characterized by the hydrophobic steroid ring ensures ~~a~~ strong interaction and intercalation with the nanosheets (Bukhari et al., 2021). In the case of polyphenols (i.e., *Ea*, *Ct* and *Ta*), the phenolic hydroxyl groups give rise to a coordination effect with the metal atoms, further stabilizing the nanosheets (Rojas et al., 2022; Zhao et al., 2019). On the other hand, the compounds' polar moieties (hydroxyl/carboxyl groups and phenolic hydroxyl groups) interact with water, mainly via hydrogen bonds, allowing MX_2 nanosheets to remain dispersed, avoiding re-stacking phenomena.

Fig. 1A reports the picture of the 16 MX_2 prepared dispersions, where each TMD (MoS_2, $MoSe_2$, WS_2 and WSe_2) was successfully exfoliated using the 4 organic compounds (*Ch*, *Ea*, *Ct* and *Ta*).

The dispersions have no visible particles and/or precipitates and show the typical color associated with the successfully exfoliated TMDs. Properly exfoliated two-dimensional TMDs possess peculiar optical properties related to the light−matter interaction due to their reduced dimensionality. Fig. S1 reports the absorption spectra of the 16 MX_2 that prove the successful exfoliation of the TMDs (Synnatschke et al., 2019); the characteristic exciton peaks at 613 ± 2/675 ± 3 (MoS_2), 632 ± 2 (WS_2), 702 ± 5 ($MoSe_2$) and 760 ± 1 nm (WSe_2) are visible independently of the compound employed as stabilizer. Noteworthy, the MX_2 dispersions remain stable for 1 year without significant aggregation/-precipitation. As control, the exfoliation has been attempted with the 4 bulk TMDs without organic compounds; no stable dispersions were obtained and the solutions resulted pale grey with precipitate (data not shown).

The SEM micrographs of the four MoS_2 reported in Fig. 1B–E confirm that nanosheets with lateral sizes of a few hundred nanometers are obtained. For all TMDs, the lateral size was significantly reduced compared to the respective bulk starting material (data not shown), where micrometric thick crystals are present (Rojas et al., 2020). Interestingly, the surface of the nanosheet appears rough and wrinkled, suggesting an interaction with the compound employed; the incorporation of the compounds onto the TMDs surface with the partial retention of the functional groups was recently demonstrated by our group (Rojas et al., 2022).

3.2. VOCs detection using 2D MX_2-based sensors

The 16 MX_2 were challenged as sensing materials for gas QCM piezoelectric sensors. The hypothesis was that the functionalization of TMDs surfaces with the organic compounds may lead to different gas sensing proprieties for VOCs given by the combination of the materials. To select the optimal nanosheet amount for QCMs, different amounts of MX_2 colloidal dispersions were tested. The piezoelectric signals (frequency shift: Δf, Hz) obtained with *Ch*-MoS_2 and *Tn*-MoS_2 used as model sensors are reported, tests were carried with 1-pentanol and isopentyl acetate (Fig. S2). The maximum loadable amount of MX_2 that returns an increase in the signal is 2 μg. This result was obtained for both sensors: every 10 μL of material added, from a dispersion at 50 mg L^{-1}, led to a response increase of approx 10–15 Hz. The procedure was extremely reproducible (Δf RSD ≤4.9%, n = 3), both for the material homogeneity and for the well-known strong affinity between TMDs and gold surface that drives the QCM functionalization.

All the 16 combinations of TMDs-organic compounds were tested selecting eight different VOCs as analytes belonging to four different chemical classes, i.e., alcohols (1-pentanol, 2-methyl-1-propanol), aldehydes (butyraldehyde, hexanal), esters (isopentyl acetate, ethyl-2-methylbutirrate), and terpenes (S-limonene, R-limonene). The selected VOCs are of particular interest since widely found in natural products and foods, and often their relative content defines an 'aroma barcode' potentially able to return information for quality, ripeness, shelf-life, and production process (Sara Gaggiotti et al., 2020).

The piezoelectric signals obtained using 1-pentanol, R-limonene, isopentyl acetate and butyraldehyde as class representative VOCs are reported in Fig. 2.

For each VOC, the sensors return an improved signal compared with

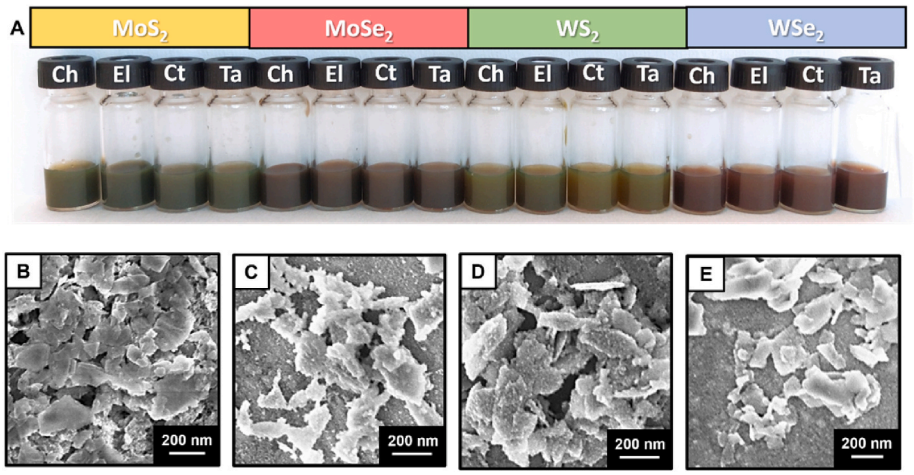

Fig. 1. MX_2 dispersions at 50 mg L^{-1} obtained with the different organic compounds (**A**). SEM micrographs of *Ch*-MoS_2 (**B**), *El*-MoS_2 (**C**), *Ct*-MoS_2 (**D**), and *Tn*-MoS_2 (**E**) at the same magnification (100 kX).

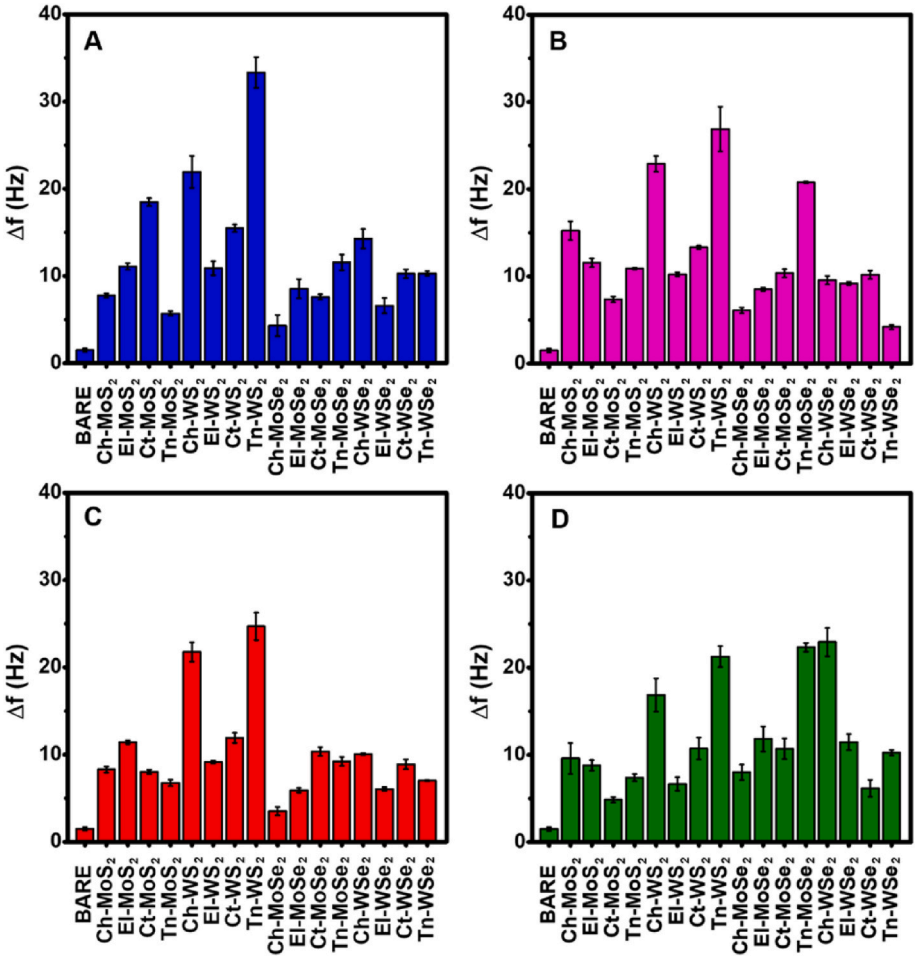

Fig. 2. QCM-MX_2 sensors frequency shifts obtained with 1-pentanol (**A**), R-limonene (**B**), isopentyl acetate (**C**), butyraldehyde (**D**). The measures were performed with an 80 cm loop.

the bare QCM, and the responses are repeatable (Δf RDS $\leq$9.5%, n = 3). The response of each sensor is different for different VOCs and, more interestingly, the 16 sensors return significantly different signals analyzing the same VOC, demonstrating the synergic effect of the MX_2 and the organic compounds used for the recognition ability. As expected, and exploited for other gas sensors, this relative affinity can be the basis for the development of gas sensor arrays (electronic noses). The data demonstrate for the first time how liquid-phase exfoliated TMDs can improve QCM piezoelectric gas sensors response, allowing modulation of the VOCs interaction dependent on the nature of TMD employed.

To investigate the MX_2-based QCM's ability to return quantitative

information, the relationship between VOC concentrations and sensors' response was studied. The frequency shifts were plotted toward the VOC concentrations. This was achieved using gas-tight PVC loops with different volumes (same diameter but different length), evaporating known quantities of solvent at a controlled temperature. Despite this way to estimate VOCs has been already reported for gas sensors (Salimi and Milani Hosseini, 2021; She et al., 2021), for the sake of clarity, it is correct to underline that VOCs have been measured in air. Fig. 3 reports the sensorgram obtained with *Tn*-WS_2 as a model sensor injecting increasing amounts of isopentyl acetate.

The response increases up to reach a plateau at ≥175 ppm, linearity was found in the 35–140 ppm range ($y = 0.093x+11.337$; $R^2 = 0.977$). A limit of detection of 5 ppm was obtained using the formula LOD = 3 S.D./m, where S.D. is the standard deviation of the intercept and m is the slope of the calibration curve. The MX_2 active role in the detection is proved in Fig. 3; in fact, it is possible to notice how for the bare QCM (black line) a significantly smallest signal, independent on VOCs amount, was obtained.

Dose-response curves for the Tn-WS_2 sensor for 1-pentanol, R-limonene, and butyraldehyde are reported in Fig. S3. The different reactivity obtained for the whole set of MX_2-based sensors towards alcohols (1-pentanol, 2-methyl-1-propanol), aldehydes (butyraldehyde, hexanal), esters (isopentyl acetate, ethyl-2-methylbutirrate), and terpenes (S-limonene, R-limonene) can be appreciated in Table 1; the sensitivity calculated from the linear portion of the respective dose-response curve is reported for all the tested materials.

For the majority of the VOCs tested R^2 of the linear range was ≥0.978. Only in few cases (6 out of 128) the sensors do not respond quantitatively to VOCs, this behavior is indicated in Table 1 with the symbol '-'. The different responses are evident looking at VOC of the same class; for instance 1-pentanol vs. 2-methyl-1-propanol, or butyraldehyde vs. hexanal, and isopentyl acetate vs. ethyl-2-methyl butyrate. The extreme variability of interaction VOCs/sensors is noticeable also for the structural isomers S-limonene and R-limonene.

The reproducibility of both MX_2 exfoliation and sensor functionalization was checked by modifying different QCMs with different batches of MX_2 dispersions. This test was performed using MoS_2- and WS_2-based sensors exfoliated with the four organic compounds, with isopentyl acetate as model VOC. An acceptable inter-sensor reproducibility (Δf RSD ≤12.8%, n = 3) proves the robustness of both TMDs exfoliation and QCM modification strategy.

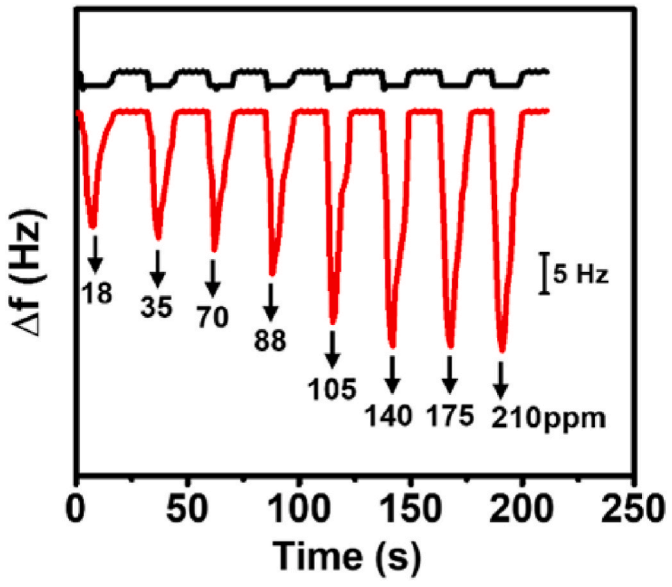

Fig. 3. Sensorgrams obtained measuring increasing concentrations of isopentyl acetate. Black-line: bare-QCM; red-line: *Tn*-WS_2 modified QCM.

Eventually, considering that signal drifting and baseline recovery after measurement represent issues that can limit the QCM-based gas sensors' use (Sara Gaggiotti et al., 2020), consecutive measures were run using 1-pentanol, R-limonene, isopentyl acetate, and butyraldehyde (see sensorgrams in Fig. S4). The results evidence that the signal for all the sensors is not affected by signal drift; the results are repeatable (Δf RSD ≤9.3%, n = 5) and the signal recovery is complete and occurs in <100 s. The sensors' response repeatability over time was tested analyzing two VOCs (isopentyl acetate and butyraldehyde) for three consecutive months, while the sensors' storage test was carried out at room temperature in the dark. In Fig. S5 is possible to appreciate how no significant response changes (Δf RSD ≤14.6%, n = 3) have been observed during this period.

It should be considered that the different response of the sensors is modulated by the TMD chemistry, enhanced by the nano-structuration that maximize the exposed surface, as well as by the organic compound laying on the surface that interacts with VOCs. The relevance of the nanomaterial/organic compound combination in piezoelectric gas sensor arrays has been already demonstrated for peptides immobilized on Au and ZnO nanoparticles and aptameric DNA structures on gold (Marcello Mascini et al., 2019; 2018). It should be noticed that, in this case, functionalization of the nanomaterial takes place during the production of the nanomaterial, thus, the density and structure of organic moieties interacting with VOCs are hard to be determined. However, the low cost, ease and sustainability of the synthesis procedure of the nanomaterial, and a large number of organic compounds potentially working as exfoliating agents may lead to a huge number of combinations to be exploited in gas sensing.

3.3. 2D MX_2-based E-nose. Banana aroma evolution monitoring as proof of concept

Fruit ripening is an irreversible process that involves a series of physiological, biochemical, and organoleptic changes; the post-harvest ripening of bananas is characterized by changes in the aroma profile (Maduwanthi and Marapana, 2019; Saraiva et al., 2018; Zhu et al., 2018). In particular, three different classes of maturation stage are recognized looking at volatile compounds' evolution: green, turning and fully ripe. During maturation, the relative amount of esters increases significantly from green to turning and then, remains constant; on the contrary, alcohols decrease rapidly and have a slight increase during ripening. The relative amount of aldehydes is reported to decrease with a rapid decay switching from the turning to the fully ripe stage (Facundo et al., 2012; Zhu et al., 2018). During the transport and storage for marketing bananas exchanges gas with the atmosphere; post-harvest ripening takes place in this way. On the other hand, pre-marketing maturation often takes place in cells with a controlled atmosphere. To simulate the ripening for marketing, bananas belonging to the same lot collected at the same time were stored at room temperature. A dedicated bunch was used for each sample collected since the ripening of the whole bunch is different from that of single bananas (since ripening is fast). For each sampling, three bananas from the same bunch were randomly selected, and three different 3 g aliquots each were collected. The samples were measured in triplicate according to *section 2.3*. The full MX_2 sensor array has been challenged by measuring each day for 10 days the bananas' aroma.

Fig. 4 reports the sensorgrams of the full set of 16 MX_2-sensors (Fig. 4A MoS_2 and WS_2 sensors; Fig. 4B $MoSe_2$ and WSe_2 sensors), for samples measured at day 1 (t_0), 5 (t_5), and 10 (t_{10}) of storage.

It is possible to appreciate signals with low noise and without significant drifts; in addition, reproducible results were obtained (Δf RSD 3.5–21.2%, n = 3). In this case, the signal is recovered in approximately 200 s.

Given the complexity of the banana aroma, single sensors' signal univariate evaluations are not practicable (Facundo et al., 2012; Saraiva et al., 2018). The whole signal database obtained over the 10 days was

Table 1
QCM-MX_2 sensitivity (Δf/[VOC]) for the studied VOCs.

QCM-MX_2	1-pentanol	2-methyl-1-propanol	Butyraldehyde	Hexanal	Isopentyl acetate	Ethyl-2-metylbutirrate	S-limonene	R-limonene
***Ch*-MoS_2**	57.8	33.1	81.9	–	60.7	–	53.8	147.2
***El*-MoS_2**	74.8	73.3	55.6	63.3	161.1	39.0	79.1	81.8
***Ct*-MoS_2**	140.4	39.2	24.5	46.4	58.2	34.8	62.3	–
***Tn*-MoS_2**	19.9	65.7	33.9	68.8	16.1	43.3	57.7	97.3
***Ch*-$MoSe_2$**	26.0	52.0	69.7	75.7	22.3	35.2	47.4	37.9
***El*-$MoSe_2$**	64.9	89.8	116.8	69.7	35.8	76.5	70.1	69.2
***Ct*-$MoSe_2$**	60.0	98.6	123.8	78.8	69.9	80.8	112.4	94.9
***Tn*-$MoSe_2$**	57.4	136.9	147.7	108.9	51.9	118.2	79.5	83.0
***Ch*-WS_2**	187.5	37.4	66.8	–	200.7	–	178.8	197.3
***El*-WS_2**	44.3	33.8	38.9	37.9	72.5	46.0	61.9	89.8
***Ct*-WS_2**	115.9	37.4	36.6	141.1	56.1	107.6	95.4	92.4
***Tn*-WS_2**	159.2	39.3	124.1	–	93.4	32.0	196.6	160.2
***Ch*-WSe_2**	67.5	129.9	182.7	43.6	57.5	42.4	147.2	76.3
***El*-WSe_2**	34.8	87.0	117.9	85.3	16.8	46.7	52.0	76.3
***Ct*-WSe_2**	63.8	47.5	26.4	45.9	53.4	40.9	94.0	51.7
***Tn*-WSe_2**	50.8	25.5	43.6	–	44.9	66.1	66.6	21.7

Dose-response curve slope: (Hz/[ppm]) x 10^3

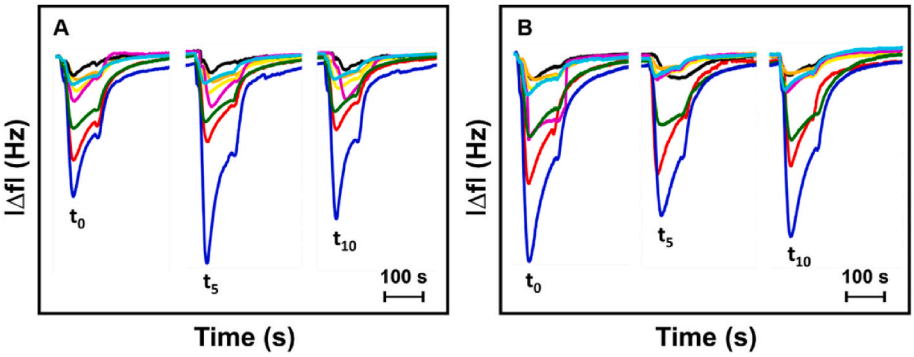

Fig. 4. Frequency shifts recorded with the full QCM-MX_2 sensor array for banana samples at different storage stages: first day (t_0), fifth day (t_5), and tenth day (t_{10}). The measures were performed with an 80 cm loop. The frequencies reported were normalized against the respective higher value. (**A**) Sensorgrams for QCM-MoS_2/WS_2 sensors: *Ch*-MoS_2 (black line), *El*-MoS_2 (green line), *Ct*-MoS_2 (orange line), *Tn*-MoS_2 (yellow line), *Ch*-WS_2 (red line), *El*-WS_2 (light blue line), *Ct*-WS_2 (purple line), *Tn*-WS_2 (blue line). (**B**) Sensorgrams for QCM-$MoSe_2$/WSe_2 sensors: *Ch*-$MoSe_2$ (Black line), *El*-$MoSe_2$ (purple line), *Ct*-$MoSe_2$ (orange line), *Tn*-$MoSe_2$ (green line), *Ch*-WSe_2 (yellow line), *El*-WSe_2 (light blue line), *Ct*-WSe_2 (red line), *Tn*-WSe_2 (blue line).

analyzed to test the discrimination ability of the sensor array. The Δf responses were then normalized and processed by PCA; the obtained loading plot (**A**) and score plot (**B**) are reported in Fig. 5.

The first two principal components explain 50.9% of the cumulative variance. In the loadings plot (Fig. 5A) it is possible to appreciate the contribution of each sensor in the discrimination of banana aroma evolution. The sensors are distributed in all 4 quadrants; this behavior confirms that all TMDs and organic compounds chemistry influence the interaction with VOCs, driving peculiar responses able to maximize the variance. In detail, a net separation among MoS_2 (upper quadrants) and WS_2 (lower quadrants) based sensors are observed; the WSe_2-sensors are all distributed in the right part of the graph (quadrants I and IV). Despite the main discrimination among sensors looks driven by the TMD, *Tn*-MX_2 sensors' partial clustering is obtained in quadrant IV. In conclusion there is no prevailing chemistry between materials and stabilizing agents (organic compounds) and, as hypothesized for the response achieved for pure compounds, also in the case of mixtures, the combination of the 2 components drives the interaction with the VOCs.

Fig. 5B reports the score plot where three clusters of samples stand out. The first cluster (purple circle) is in the right part of the graph (I and IV quadrants) and contains samples measured within 4 days of storage and corresponding to the green stage; in fact, bananas are green and appear unripe. The second group (orange circle), localized in the III quadrant, is constituted by samples on the 5-6th day of storage (bananas turn yellow). Brown spots on the samples corresponding to the last stage of storage (ripe) are grouped in the II quadrant (green circle). This

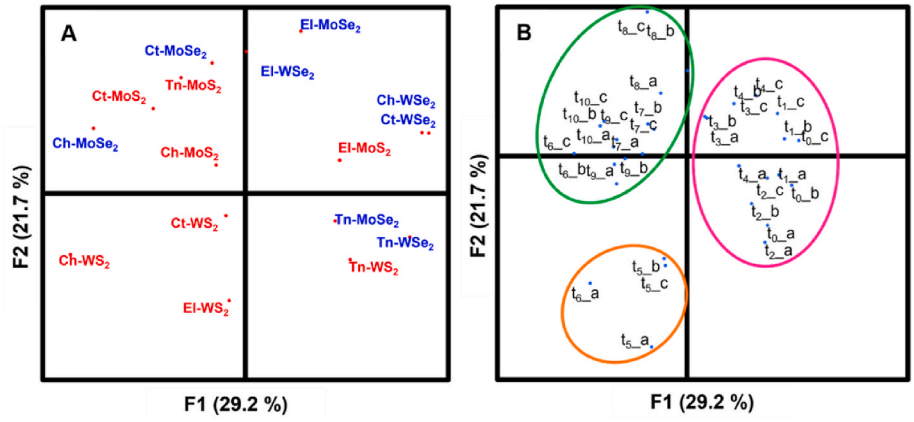

Fig. 5. PCA loadings plot (**A**) and scores plot (**B**), obtained analyzing the frequency shifts recorded with the QCM-MX_2 sensor array for the banana samples storage study. Plots of the first two components (explained variance: PC1 = 29.2.0%; PC2 = 21.7%; total = 50.9%). (**A**) In the loading plot, the QCM-MoS_2/WS_2 are reported in red, and the QCM-$MoSe_2$/WSe_2 in blue. (**B**) In the score plot, the banana samples at different storage times are reported (from t_0 to t_{10}), and for each storage day, the average value of banana samples from three different bunches (indicated as a, b, and c) are reported. The three bananas samples groups found are highlighted with circles of different colors.

confirms the findings reported by other authors (Facundo et al., 2012; Saraiva et al., 2018; Sonmezdag et al., 2014; Zhu et al., 2018).

These data indicate that 2D MX_2 are new interesting sensing elements for piezoelectric gas sensor arrays (e-noses) that allow QCMs to respond quantitatively to different classes of VOCs. Moreover, thanks to the combination of TMDs and stabilizing agents it is possible to implement sensor arrays able to monitor aroma differences and evolution in complex real matrices.

4. Conclusions

In this work, Group VI transition metal dichalcogenides functionalized with organic compounds are successfully proposed as new sensing elements for QCM gas sensors. These materials, obtained via LPE in water, resulted nanostructured, with a 2D few-layer conformation, stable and easy to handle. The combination of four TMDs and four organic compounds was used to produce 16 sensors that have been tested towards different classes of VOCs and real samples. The sensors showed a linear relationship between the piezoelectric frequency shift and the VOC concentrations, allowing VOCs quantification in model systems. Furthermore, given the different sensitivity toward VOCs of the 16 sensors, they were used in an array format to equip an e-nose, that was challenged to monitor bananas ripening. The combination of different TMDs functionalized with different organic molecules, gives rise to functional materials that strategically allow boosting and modulating gas sensor receptors' features. This work provides the basis to stimulate the use of water-phase exfoliated TMDs with organic molecules to develop sensitive, reproducible, and stable gas sensors with modulable interaction towards VOCs, throughout a sustainable and within everyone's reach synthesis.

Declaration of competing interest

The authors declare that they have no known competing financial interests or personal relationships that could have appeared to influence the work reported in this paper.

Data availability

No data was used for the research described in the article.

Acknowledgments

DC, SG, and AC acknowledges the PSR ABRUZZO 2014e2020 SM 16.2 "Sostegno a progetti pilota e allo sviluppo di nuovi prodotti, pratiche, processi e tecnologie. Progetto Innovaolio".

FDP and DC acknowledge the Ministry of Education, University and Research (MIUR) and European Social Fund (ESF) for the PON R&I 2014–2020 program, action 1.2 ′AIM: Attraction and International Mobility' (AIM1894039-3).

GF acknowledges the Italian Ministry of Education, University and Research (MIUR) and European Social Fund (ESF) for the PON R&I 2014–2020 program, action IV.6 'Research contracts on green issues' and acknowledge partial financial support from Consorzio per lo sviluppo dei Sistemi a Grande Interfase (CSGI).

Appendix A. Supplementary data

Supplementary data to this article can be found online at https://doi.org/10.1016/j.bios.2022.114749.

References

Brenet, S., John-Herpin, A., Gallat, F.X., Musnier, B., Buhot, A., Herrier, C., Rousselle, T., Livache, T., Hou, Y., 2018. Highly-selective optoelectronic nose based on surface plasmon resonance imaging for sensing volatile organic compounds. Anal. Chem. 90, 9879–9887. https://doi.org/10.1021/acs.analchem.8b02036.

Bukhari, Q.U.A., Silveri, F., Della Pelle, F., Scroccarello, A., Zappi, D., Cozzoni, E., Compagnone, D., 2021. Water-phase exfoliated biochar nanofibers from Eucalyptus scraps for electrode modification and conductive film fabrication. ACS Sustain. Chem. Eng. 9, 13988–13998. https://doi.org/10.1021/acssuschemeng.1c05893.

D'Amico, A., Di Natale, C., Paolesse, R., Macagnano, A., Mantini, A., 2000. Metalloporphyrins as basic material for volatile sensitive sensors. Sensor. Actuator. B Chem. 65, 209–215. https://doi.org/10.1016/S0925-4005(99)00342-1.

Facundo, H.V.de V., Garruti, D., dos, S., Dias, C.T., dos, S., Cordenunsi, B.R., Lajolo, F.M., 2012. Influence of different banana cultivars on volatile compounds during ripening in cold storage. Food Res. Int. 49, 626–633. https://doi.org/10.1016/j.foodres.2012.08.013.

Fauzi, F., Rianjanu, A., Santoso, I., Triyana, K., 2021. Gas and humidity sensing with quartz crystal microbalance (QCM) coated with graphene-based materials – a mini review. Sensors Actuators, A Phys. 330, 112837 https://doi.org/10.1016/j.sna.2021.112837.

Gaggiotti, S., Mascini, M., Pittia, P., Pelle, F.D., Compagnone, D., 2019. Headspace volatile evaluation of carrot samples-comparison of GC/MS and AuNPs-hpDNA-Based E-Nose. Foods 8. https://doi.org/10.3390/foods8080293.

Gaggiotti, S., Palmieri, S., Della Pelle, F., Sergi, M., Cichelli, A., Mascini, M., Compagnone, D., 2020. Piezoelectric peptide-hpDNA based electronic nose for the detection of terpenes; Evaluation of the aroma profile in different Cannabis sativa L. (hemp) samples. Sensor. Actuator. B Chem. 308 https://doi.org/10.1016/j.snb.2020.127697.

Gaggiotti, S., Della Pelle, F., Mascini, M., Cichelli, A., Compagnone, D., 2020. Peptides, DNA and MIPs in gas sensing. From the realization of the sensors to sample analysis. Sensors 20, 1–28. https://doi.org/10.3390/s20164433.

Ghatak, S., Pal, A.N., Ghosh, A., 2011. Nature ofElectronic states in atomically thin MoS2 field-effect transistors. ACS Nano 7707–7712. https://doi.org/10.1021/nn202852j.

Grayfer, E.D., Kozlova, M.N., Fedorov, V.E., 2017. Colloidal 2D nanosheets of MoS2 and other transition metal dichalcogenides through liquid-phase exfoliation. Adv. Colloid Interface Sci. 245, 40–61. https://doi.org/10.1016/j.cis.2017.04.014.

Ko, K.Y., Song, J.G., Kim, Y., Choi, T., Shin, S., Lee, C.W., Lee, K., Koo, J., Lee, H., Kim, J., Lee, T., Park, J., Kim, H., 2016. Improvement of gas-sensing performance of large-area tungsten disulfide nanosheets by surface functionalization. ACS Nano 10, 9287–9296. https://doi.org/10.1021/acsnano.6b03631.

Kumar, R., Goel, N., Hojamberdiev, M., Kumar, M., 2020. Transition metal dichalcogenides-based flexible gas sensors. Sensors Actuators, A Phys. 303, 111875 https://doi.org/10.1016/j.sna.2020.111875.

Maduwanthi, S.D.T., Marapana, R.A.U.J., 2019. Comparative study on aroma volatiles, organic acids, and sugars of ambul banana (musa acuminata, AAB) treated with induced ripening agents, 2019 J. Food Qual. 1–9. https://doi.org/10.1155/2019/7653154.

Mascini, M., Gaggiotti, S., Della Pelle, F., Natale, C.D., Qakala, S., Iwuoha, E., Pittia, P., Compagnone, D., 2018. Peptide modified ZnO nanoparticles as gas sensors array for volatile organic compounds (VOCs). Front. Chem. 6 https://doi.org/10.3389/fchem.2018.00105.

Mascini, M., Gaggiotti, S., Della Pelle, F., Natale, C.Di, Qakala, S., Iwuoha, E., Pittia, P., Compagnone, D., 2018. Peptide modified ZnO nanoparticles as gas sensors array for volatile organic compounds (VOCs). Front. Chem. 6, 1–9. https://doi.org/10.3389/fchem.2018.00105.

Mascini, M., Gaggiotti, S., Della Pelle, F., Wang, J., Pingarrón, J.M., Compagnone, D., 2019. Hairpin DNA-AuNPs as molecular binding elements for the detection of volatile organic compounds. Biosens. Bioelectron. 123 https://doi.org/10.1016/j.bios.2018.07.028.

Mascini, M., Gaggiotti, S., Della Pelle, F., Wang, J., Pingarrón, J.M., Compagnone, D., 2019. Hairpin DNA-AuNPs as molecular binding elements for the detection of volatile organic compounds. Biosens. Bioelectron. 123, 124–130. https://doi.org/10.1016/j.bios.2018.07.028.

Mascini, M., Pizzoni, D., Perez, G., Chiarappa, E., Di Natale, C., Pittia, P., Compagnone, D., 2017. Tailoring gas sensor arrays via the design of short peptides sequences as binding elements. Biosens. Bioelectron. https://doi.org/10.1016/j.bios.2016.09.028.

Paczkowski, S., Nicke, S., Ziegenhagen, H., Schütz, S., 2015. Volatile emission of decomposing pig carcasses (Sus scrofa domesticus L.) as an indicator for the postmortem interval. J. Forensic Sci. 60, S130–S137. https://doi.org/10.1111/1556-4029.12638.

Paredes, J.I., Villar-Rodil, S., 2016. Biomolecule-assisted exfoliation and dispersion of graphene and other two-dimensional materials: a review of recent progress and applications. Nanoscale 8, 15389–15413. https://doi.org/10.1039/c6nr02039a.

Rojas, D., Della Pelle, F., Del Carlo, M., Compagnone, D., Escarpa, A., 2020. Group VI transition metal dichalcogenides as antifouling transducers for electrochemical oxidation of catechol-containing structures. Electrochem. Commun. 115, 106718 https://doi.org/10.1016/j.elecom.2020.106718.

Rojas, D., Della Pelle, F., Silveri, F., Ferraro, G., Fratini, E., Compagnone, D., 2022. Phenolic compounds as redox-active exfoliation agents for group VI transition metal dichalcogenides. Mater. Today Chem. 26, 101122. https://doi.org/10.1016/j.mtchem.2022.101122.

Rojas, D., Hernández-Rodríguez, J.F., Della Pelle, F., Escarpa, A., Compagnone, D., 2022. New trends in enzyme-free electrochemical sensing of ROS/RNS. Application to live cell analysis. Mikrochim. Acta 189, 102. https://doi.org/10.1007/s00604-022-05185-w.

Salimi, M., Milani Hosseini, S.M.R., 2021. Smartphone-based detection of lung cancer-related volatile organic compounds (VOCs) using rapid synthesized ZnO nanosheet. Sensor. Actuator. B Chem. 344, 130127 https://doi.org/10.1016/j.snb.2021.130127.

Samadi, M., Sarikhani, N., Zirak, M., Zhang, H., Zhang, H.L., Moshfegh, A.Z., 2018. Group 6 transition metal dichalcogenide nanomaterials: synthesis, applications and future perspectives. Nanoscale Horizons 3, 90–204. https://doi.org/10.1039/c7nh00137a.

Saraiva, L.A., Castelan, F.P., Gomes, B.L., Purgatto, E., Cordenunsi-Lysenko, B.R., 2018. Thap Maeo bananas: fast ripening and full ethylene perception at low doses. Food Res. Int. 105, 384–392. https://doi.org/10.1016/j.foodres.2017.11.007.

Sayago, I., Aleixandre, M., Santos, J.P., 2019. In: Development of Tin Oxide-Based Nanosensors for Electronic Nose Environmental Applications. https://doi.org/10.3390/bios9010021. Biosensors.

She, C., Li, G., Zhang, W., Xie, G., Zhang, Y., Li, L., Yue, F., Liu, S., Jing, C., Cheng, Y., Chu, J., 2021. A flexible polypyrrole/silk-fiber ammonia sensor assisted by silica nanosphere template. Sensors Actuators, A Phys. 317, 112436 https://doi.org/10.1016/j.sna.2020.112436.

Silveri, F., Della Pelle, F., Rojas, D., Bukhari, Q.U.A., Ferraro, G., Fratini, E., Compagnone, D., 2021. (+)-Catechin-assisted graphene production by sonochemical exfoliation in water. A new redox-active nanomaterial for electromediated sensing. Microchim. Acta 188. https://doi.org/10.1007/s00604-021-05018-2.

Silveri, F., Della Pelle, F., Scroccarello, A., Ain Bukhari, Q.U., Del Carlo, M., Compagnone, D., 2022. Modular graphene mediator film-based electrochemical pocket device for chlorpyrifos determination. Talanta 240. https://doi.org/10.1016/j.talanta.2022.123212.

Sonmezdag, A.S., Kelebek, H., Selli, S., 2014. Comparison of the aroma and some physicochemical properties of grand naine (musa acuminata) banana as influenced by natural and ethylene-treated ripening. J. Food Process. Preserv. 38, 2137–2145. https://doi.org/10.1111/jfpp.12194.

Synnatschke, K., Cieslik, P.A., Harvey, A., Castellanos-Gomez, A., Tian, T., Shih, C.J., Chernikov, A., Santos, E.J.G., Coleman, J.N., Backes, C., 2019. Length- and thickness-dependent optical response of liquid-exfoliated transition metal dichalcogenides. Chem. Mater. 31, 10049–10062. https://doi.org/10.1021/acs.chemmater.9b02905.

UN General Assembly, 2015. In: Transforming Our World: the 2030 Agenda for Sustainable Development.. New York: United Nations. http://www.un.org/ga/search/view_doc.asp?symbol=A/RES/70/1&Lang=E.

Wang, L., 2020. Review of gravimetric sensing of volatile organic compounds. Sensors Actuators, A Phys. 307, 111984 https://doi.org/10.1016/j.sna.2020.111984.

Wang, Q.H., Kalantar-Zadeh, K., Kis, A., Coleman, J.N., Strano, M.S., 2012. Electronics and optoelectronics of two-dimensional transition metal dichalcogenides. Nat. Nanotechnol. 7, 699–712. https://doi.org/10.1038/nnano.2012.193.

Zhang, J., Liu, L., Yang, Y., Huang, Q., Li, D., Zeng, D., 2021. A review on two-dimensional materials for chemiresistive- and FET-type gas sensors. Phys. Chem. Chem. Phys. 23, 15420–15439. https://doi.org/10.1039/d1cp01890f.

Zhang, S., Wang, J., Torad, N.L., Xia, W., Aslam, M.A., Kaneti, Y.V., Hou, Z., Ding, Z., Da, B., Fatehmulla, A., Aldhafiri, A.M., Farooq, W.A., Tang, J., Bando, Y., Yamauchi, Y., 2020. Rational design of nanoporous MoS2/VS2 heteroarchitecture for ultrahigh performance ammonia sensors. Small 16, 1–9. https://doi.org/10.1002/smll.201901718.

Zhao, H., Wu, H., Wu, J., Li, J., Wang, Y., Zhang, Y., Liu, H., 2019. Preparation of MoS2/WS2 nanosheets by liquid phase exfoliation with assistance of epigallocatechin gallate and study as an additive for high-performance lithium-sulfur batteries. J. Colloid Interface Sci. 552, 554–562. https://doi.org/10.1016/j.jcis.2019.05.080.

Zhu, X., Li, Q., Li, J., Luo, J., Chen, W., Li, X., 2018. Comparative study of volatile compounds in the fruit of two banana cultivars at different ripening stages. Molecules 23, 2465. https://doi.org/10.3390/molecules23102456.